Appl. Phys. A 67, 557–561 (1998)

Applied Physics A
Materials
Science & Processing

Prompt electron emission and collisional ionization of ambient gas during pulsed laser ablation of silver

R.C. Issac, G.K. Varier, P. Gopinath, S.S. Harilal, V.P.N. Nampoori, C.P.G. Vallabhan

Laser Division, International School of Photonics, Cochin University of Science & Technology, Cochin 682 022, India
(E-mail: photonix@md2.vsnl.net.in)

Received: 5 January 1998/Accepted: 3 July 1998

Abstract. A silver target kept under partial vacuum conditions was irradiated with focused nanosecond pulses at 1.06 μm from a Nd:YAG laser. The electron emission monitored with a Langmuir probe shows a clear twin-peak distribution. The first peak which is very sharp has only a small delay and it indicates prompt electron emission with energy as much as 60 ± 5 eV. Also the prompt electron emission shows a temporal profile with a width that is same as that for the laser pulse whereas the second peak is broader, covers several microseconds, and represents the low-energy electrons (2 ± 0.5 eV) associated with the laser-induced silver plasma as revealed by time-of-flight measurements. It has been found that prompt electrons ejected from the target collisionally excite and ionize ambient gas molecules. Clearly resolved rotational structure is observed in the emission spectra of ambient nitrogen molecules. Combined with time-resolved spectroscopy, the prompt electrons can be used as excitation sources for various collisional excitation–relaxation experiments. The electron density corresponding to the first peak is estimated to be of the order of 10^{17} cm^{-3} and it is found that the density increases as a function of distance away from the target. Dependence of probe current on laser intensity shows plasma shielding at high laser intensities.

PACS: 52.50.J; 52.40.N; 52.75.R; 34.80.D; 39.90

With the invention of the high-power pulsed lasers, the study of laser–matter interactions has assumed many new dimensions among which the phenomenon of laser ablation has a major role both in fundamental studies and in technological applications [1–4]. The interaction of laser radiation with solids is a very complex process. It includes light absorption and plasma formation in the vicinity of the target [5], thermalisation of the ablation products due to collisions among themselves and with ambient gas molecules [6–9], evolution and propagation of the plume [10–13], gas phase chemical reactions [14, 15], and the eventual deposition of the ablative products on suitable substrates situated at a distance from the target [1, 2]. In metals, laser absorption occurs within the skin depth because of the exponential attenuation of electromagnetic radiation in a conducting medium. The light is primarily absorbed by electrons present within the skin depth through inverse bremsstrahlung leading to rapid ionization before significant ablation of the solid occurs. The absorbed energy is transferred to the lattice through electron–phonon (e–ph) interactions which usually happens within a few picoseconds after the absorption [16]. The e–ph relaxation time increases with the laser fluence. This increase in e–ph relaxation time is due to the greater difference between electron and lattice temperatures and hence the greater number of collisions that are required for thermalisation. Most of the theoretical and observational models on laser ablation describe the formation of the plasma and its gas dynamic effects. Consequently, the hot-electron emission process during nanosecond laser interactions and its effect on the ambient gas molecules have not received much attention.

In the present paper we report the observation of high-current, high-temperature electron pulses generated during the interaction of infrared radiation from a Nd:YAG laser with a silver target. The current pulse from a positively biased Langmuir probe shows that there are two peaks in the time-of-flight (TOF) profile; one caused by the fast prompt electrons which lasts for a few nanoseconds after the laser pulse and the second appears much later in time and has a temporal width of several microseconds. The use of such initial fast electrons for the vibrational excitation and ionization of molecular nitrogen through electron impact is also demonstrated.

1 Experimental details

The schematic of the experimental setup is shown in Fig. 1. It consists of a plasma chamber fitted with rotary and diffusion pumps for evacuating the chamber, which can then be filled with the required gas at the desired pressure. The chamber has viewing ports through which the optical emission from the plasma can be monitored. There are provisions made on the chamber through which current probes can be inserted. The target to probe separation can be controlled from outside the chamber. The 1.06-μm laser beam from a Q-switched

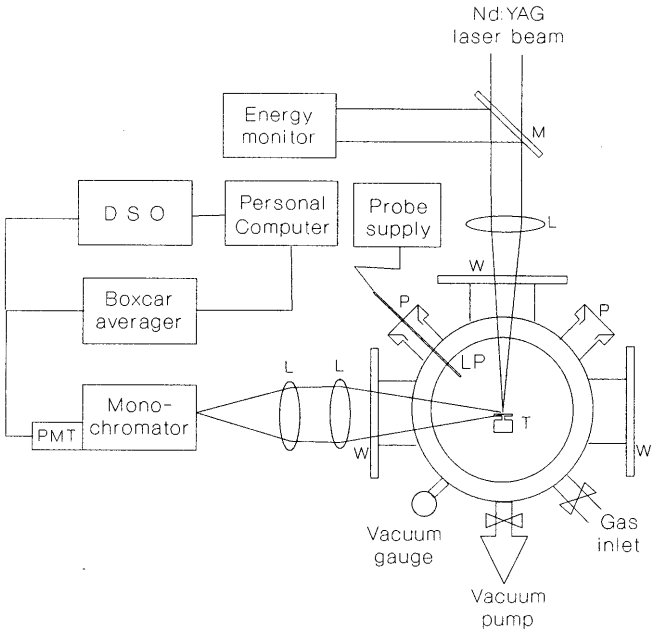

Fig. 1. Schematic of the experimental setup. M, 10% reflector; L, lens; W, glass windows; P, probe insertion port; LP, Langmuir probe; T rotating target holder; PMT, photomultiplier tube; DSO, digital storage oscilloscope. The laser spot size was 50 μm in radius

Nd:YAG laser (Quanta Ray) with pulse width (full width at half maximum) 10 ns was focused onto the polished front surface of a disc-shaped silver target (diameter 2.5 cm, thickness 0.15 cm). The laser pulses produce luminous plasma in front of the target and the plasma plume expands in a direction perpendicular to the target surface. At first sight one may think that the expansion is 3-dimensional. But since the velocity distribution is highly anisotropic and forward peaked, usually a unidirectional expansion is assumed for the plume. The target was rotated about its axis in order to avoid multiple hits at the same spot. For studies involving Langmuir probes, the target was kept at 45° to the laser beam propagation direction. The probe is positively biased through an external power supply and the transient probe current is monitored across a 50 Ω load using a digital storage oscilloscope (TDS 220, Tektronix). Such a setup gives true pulse shapes of the plasma electron current. The oscilloscope was interfaced with a personal computer (PC) for data acquisition and analysis. In all our measurements the pressure inside the chamber was kept at 27 Pa.

For time-resolved spectral measurements, the plasma plume was imaged onto the entrance slit of the monochromator provided with a thermoelectrically cooled photomultiplier tube (PMT) for detection. The spatial resolution is obtained by placing proper slits and apertures to expose various segments of the plasma. A boxcar averager (SRS 250, Stanford Research Systems) is used for gating and averaging the spectrum during time-resolved measurements. The spectra were measured with the input impedance of the boxcar averager kept at 50 Ω and the averaged output is fed to a PC for further analysis. The laser was operated at a repetition frequency of 10 Hz, and using the boxcar averager, spectral intensities were averaged out from ten successive pulses. The temporal pulse shapes of optical emission at specific wavelengths were measured directly by feeding the PMT output to the digital storage oscilloscope with a 50 Ω load.

2 Results and discussion

2.1 TOF profiles of electrons

The focused 1.06-μm radiation from the Nd:YAG laser was allowed to fall onto the silver target kept inside the partially evacuated plasma chamber. This generates a bright luminous plasma from the target surface which evolves to an elongated plume of length about 4–5 cm. We have studied the plasma evolution with the help of a Langmuir probe made up of tungsten. Most of the TOF measurements reported so far concentrated primarily on the dynamics of atoms and ions and not on the time evolution of the electrons. But in order to have a better understanding on the process of laser–matter and laser–plasma interactions it is necessary to analyze the temporal behavior of electrons also since the dynamics of electrons greatly influence the evolution of the plasma [17]. Figure 2 is the signal from a positively biased Langmuir probe. There are two distinct peaks in the current signal, the initial component comes almost simultaneously with the laser pulse and lasts only for a few ns. Following this a broad electron current signal is seen which extends over several μs. The second peak comes well after the termination of the laser pulse and its delay depends on the separation of the probe from the target surface. An enlarged profile of the fast electron peak alone is shown as an inset to Fig. 2. The temporal width is only 10 ns and almost follows the laser beam temporal profile which is Gaussian in time. The slope of the plot between the natural logarithm of the probe current and the applied probe voltage is e/kT, T being the electron temperature, e the electronic charge, and k the Boltzmann constant. The electron temperatures corresponding to both the peaks were evaluated at a distance 0.5 cm and it was found that corresponding to the

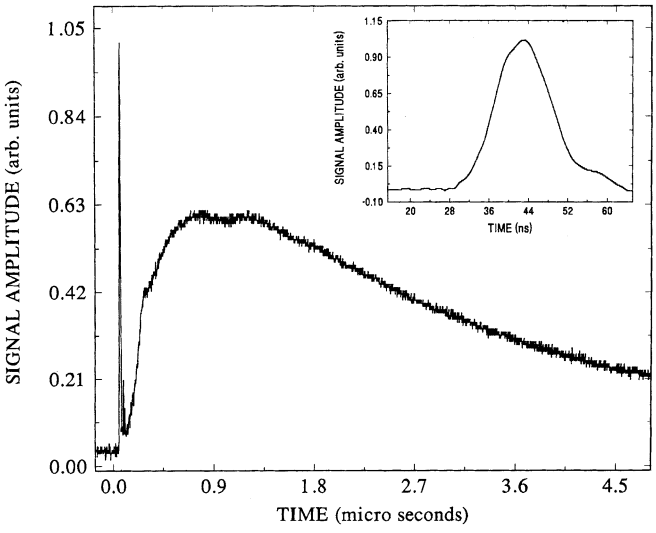

Fig. 2. Temporal profile of a positively biased probe signal at a distance 0.5 cm from the target. The profile shows twin peak distribution. The narrow peak appears early in time and represents prompt electrons and the broad peak corresponds to the plasma electrons, which extends to several μs. Inset: enlarged view of the first peak. The temporal width (FWHM) is about 10 ns, equal to that of the laser pulse width

first peak the temperature was as high as 60 ± 5 eV while that corresponding to second peak was only 2 ± 0.5 eV. Therefore the electrons in the fast peak had sufficient energy to collisionally ionize the ambient gas molecules or atoms.

The interaction of the laser pulse with a solid surface leads to its absorption by the conduction electrons in the skin depth mostly through inverse bremsstrahlung. The absorbed energy is transferred to the bulk of the material through e–ph interactions and hence the temperature rises abruptly and a high temperature plasma is formed within the thermal conduction depth, i.e. a typical depth up to which the heating is effective to produce ablation [18]. The time evolution of the electron (T_e) and lattice (T_l) temperatures are described by the coupled nonlinear differential equations [16, 19],

$$C_e(T_e)\frac{dT_e}{dt} = K\nabla^2 T_e - G(T_e - T_l) + P_a(r,t) \quad (1)$$

and

$$C_l\frac{dT_l}{dt} = G(T_e - T_l)\,, \quad (2)$$

where $C_e(T_e)$ (J/m^{3}K) is the electronic heat capacity, K (W/mK) is the thermal conductivity, G (W/m^{3}K) is the coefficient of heat transfer between the electrons and lattice, $P_a(r,t)$ is the absorbed laser power density given by $(1-R)\alpha I \exp(-\alpha z)\, f(t)$, α (m^{-1}) is the absorption coefficient, R is the reflectivity, I (W m^{-2}) is the laser intensity, $f(t)$ is the laser temporal profile, and C_l (J/m^{3}K) is the lattice heat capacity. Numerical evaluation of the temporal variations of T_e and T_l in the case of copper showed that electron heating is very fast whereas the lattice temperature rises rather slowly [16]. Eesley [20, 21] has observed non-equilibrium electron heating in copper during picosecond laser interaction due to the initial heating of electrons well above the lattice temperature. The surface electron temperature follows almost the same temporal profile as the heating laser pulse whereas the heat is transferred to the lattice with a delay in time [21]. The energy transferred to the lattice will result in bond breaking and the evaporated material forms a plasma which expands as a supersonic jet from the target surface. A fraction of the hot electrons may escape from the interaction volume before the energy gets transferred to the lattice through collisions. The first peak corresponds to such electrons escaping from the focal volume. The second peak corresponds to the plasma electrons, which exist for a longer time period. In Fig. 3 the current signal from a negatively biased Langmuir probe is given. Two distinct peaks corresponding to the ions are seen in the figure. The first peak corresponds to the current due to the local population of the ionized ambient molecules as revealed by the time-resolved spectral measurements described later in Sect. 2.2. The time delay of the first ion peak almost coincides with the prompt electron emission peak in the electron temporal profile. The second peak in the ion TOF profile follows almost the same time scale of the second peak in the electron TOF profile. Thus it can be safely inferred that the second peak in the electron TOF profile corresponds to the electrons contained in the silver plasma.

Figure 4 shows the dependence of the probe current corresponding to the first electron pulse on the laser peak intensity. The probe current increases linearly with laser intensity up to about 9.5×10^{10} W cm^{-2} and thereafter it saturates. The

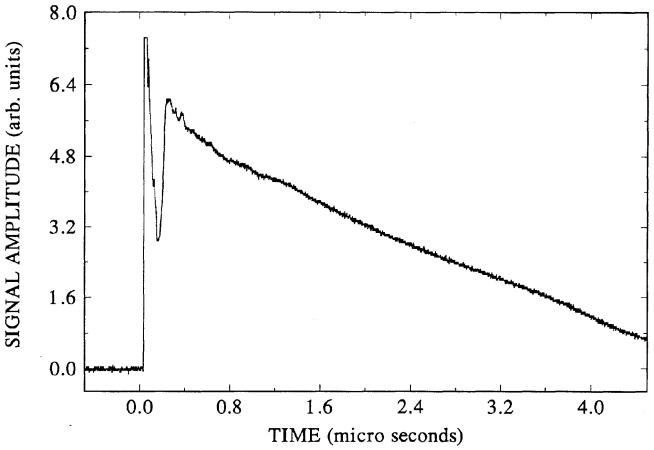

Fig. 3. The time-of-flight profile from a negatively biased probe at a distance 0.5 cm from the target. The first peak corresponds to current due to ionized nitrogen molecules and the broad peak corresponds to ions from the laser plasma

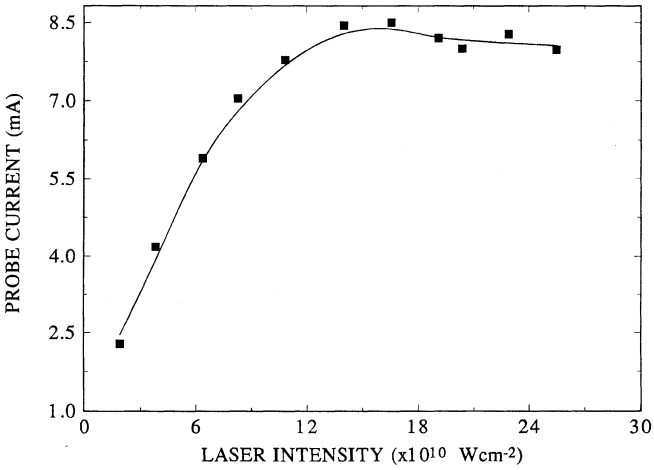

Fig. 4. Probe current for the first electron temporal peak as a function of laser intensity. The electron current increases up to a laser intensity of about 9.5×10^{10} W cm^{-2} and then saturates due to plasma shielding

surface and volume photoelectric effects through multiphoton excitation of metallic surfaces have been reported [22–24] and in such cases the electron current density (J) has a power law dependence on the input laser intensity (I). That is, $J \propto I^n$ where n is an integer such that $nh\nu$ (h is Planck's constant and ν the light frequency) coincides with or slightly exceeds the work function of the material. But in the present case n lies between 1 and 1.5, which does not match with the work function of silver [25] (4.26 eV). Therefore multiphoton photoemission may not contribute much to the prompt electron emission found in the present investigations. In an experiment with graphite as the target [26] electron kinetic energies in excess of 15 eV was observed and the electron heating was attributed to collisional absorption of laser light by free electrons through inverse bremsstrahlung. The saturation in electron current at higher laser intensities is due to plasma screening of the laser pulse. The total optical intensity available at the target is thus reduced and hence the electron number density and probe current are also reduced. Russo [27] describes the shielding of the ns laser beam during

its interaction with the pre-formed plasma as due to absorption by the atoms and ions as they expand into the gas because of the absence of free electrons. In the case of ps laser pulses, the shielding is due to absorptions by free electrons. Our observation of the saturation in the prompt electron current at higher laser intensities suggests that during ns laser interactions with metals, absorption by free electrons contributes to plasma shielding.

The electrons could be heated up by absorption of laser light by means of above-threshold ionization (ATI), electron oscillations in the laser electric field (ponderomotive potentials), or could be through to inverse bremsstrahlung absorption. During ATI there should be a number of electron peaks separated by the laser photon energy [28]. In general electron heating with lasers is described classically with the concept of ponderomotive force [29]. The electrons begin to vibrate in the varying electromagnetic field and attain a kinetic energy [28], $U = e^2E_0^2/4m\omega^2$, where E_0 is the electric field associated with the laser light, ω is the frequency of the optical field, e and m are the electron charge and mass, respectively. This ponderomotive energy is converted into kinetic energy as the electrons leave the light beam and the electrons are accelerated outwards. Thus ponderomotive forces can really play a prominent role in electron heating. High-energy electrons have been observed in ps laser interaction with solids. Electron velocities of the order of $10^9\,\mathrm{cm\,s^{-1}}$ have been reported in such instances [22]. Another heating mechanism, as mentioned above, is that due to the absorption of the laser radiation through inverse bremsstrahlung [30].

2.2 Time-resolved spectroscopy

Time-resolved spectroscopy from laser-produced plasmas has been the subject of many research articles [31, 32]. Usually in high-density laser plasmas, during initial time periods the spectrum is dominated by the continuum emission and as the plasma cools down the signatures of atomic and ionic emissions begin to appear [33]. In the present study the time-resolved spectrum is recorded and it is found that very early even before the arrival of plasma emission, the spectral emission from the ambient gas occurs under partial vacuum conditions.

The spectrum in the range 350–800 nm is recorded with the boxcar gate delay 0 ns and width 40 ns for a nitrogen ambient atmosphere. The most prominent features in the emission spectrum are due to the N_2 and N_2^+ molecular systems. A representative spectrum in the range 350 nm to 420 nm is shown in Fig. 5. The spectrum shows emission bands corresponding to N_2 and N_2^+ and does not have any emission characteristic of the silver atoms or silver ions emitted from the target. Since the ground state of N_2 is a singlet, the direct excitation to the triplet that gives rise to the second positive system is normally forbidden except through the mechanism of energy exchange [34]. A high-resolution spectrum giving the rotational fine structure with alternate half intensities of the $\Delta v = -1$ band of N_2^+ with band head at 427.8 nm is shown as an inset to Fig. 5. Such intensity alternations can be observed for homonuclear molecules due to the difference in statistical weights for even and odd numbered rotational levels. The intensity ratio is given by $(I+1)/I$ where I is the nuclear spin quantum number [35]. The nuclear spin of the

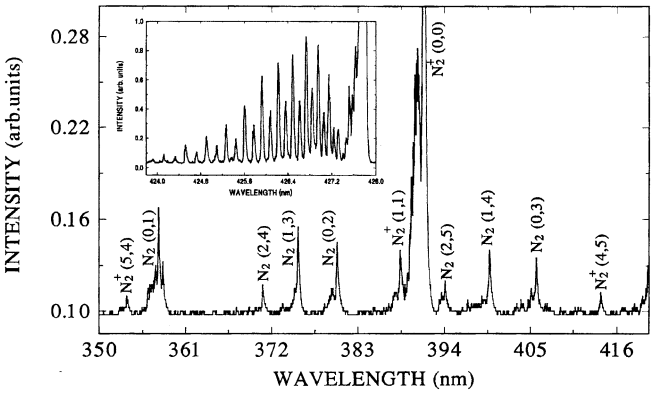

Fig. 5. Time-resolved spectrum with nitrogen as ambient medium recorded with a boxcar gate delay of 0 ns and gate width 40 ns. The spectrum shows emission from background gas molecules only and characteristic emission from silver is not seen during initial time delays. The rotational fine structure of the $\Delta v = -1$ band from N_2^+ with band head at 427.8 nm is shown as inset

N_2^{14} isotope is one and thus the intensity ratio for alternate lines should be 2 : 1. Slight deviations from 2 : 1 intensity alternations in the recorded spectrum are due to the P and R branch overlap [36, 37]. The above observations show that the laser plasma from silver is preceded by a partially ionized ambient gas plasma. Thus the density of the prompt electrons can be obtained from the Stark-broadened emission profile of the ambient gas atoms and ions [38, 39]. With an argon ambient, the medium is almost fully ionized and the spectrum is dominated by the singly ionized species as shown in Fig. 6. The density of the prompt electron pulse as a function of distance from the target is evaluated using the emission line profile from Ar II at 480.6 nm and it was found that the density increases as distance increases. The variation of the electron density with distance is shown in Fig. 7. Near the target, the electron density is $1.8 \times 10^{17}\,\mathrm{cm^{-3}}$ and at 1 cm it is $3.4 \times 10^{17}\,\mathrm{cm^{-3}}$. There is a steady increase in the electron density as distance from the target is increased. This is expected since the ionization of each argon atom produces one additional electron, i.e. $\mathrm{Ar} + \mathrm{e} \rightarrow \mathrm{Ar}^{+*} + 2\mathrm{e}$. The electron density attains a steady-state value after about 0.7 cm from the target surface.

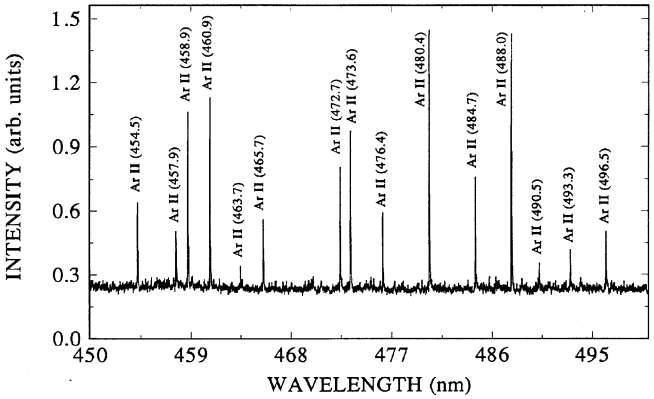

Fig. 6. The time-resolved spectrum at gate delay 0 ns and gate width 40 ns with argon as the ambient gas. The spectrum is dominated by singly ionized argon

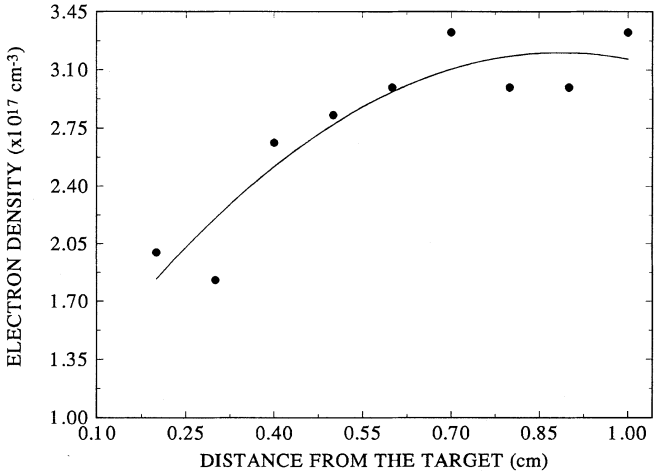

Fig. 7. Variation of prompt electron density as a function of distance from the target. The density increases with distance indicating electron generation due to collisional ionization of ambient molecules

3 Conclusions

We have described here measurements related to the production of high-energy electron pulses during ns laser interaction with a metal target. The electron pulses thus generated have been found to cause ionization and the excitation of atoms and molecules in the ambient gas. To the best of our knowledge laser-heated prompt electrons have not yet been used for ambient molecular excitation–relaxation studies in a systematic way. Electron–molecule, electron–atom collisions, ionization, and the corresponding energy transfer have acquired considerable interest in recent times. The electron–vibration (e–V) and electron–rotation (e–R) energy transfer and the determination of the corresponding rate constants assume particular importance in atmospheric science, astronomy, and in high-velocity plasma flows. Most of the studies related to the e–V energy transfer is theoretical and there is need for the development of appropriate experimental techniques to study the energy exchanges. Recently Bourden and Vervish [40] considered the anharmonicity in the molecular vibrations in nitrogen molecules and have shown that the initial values of vibrational and electron temperatures modify the behavior of energy relaxation. N_2 can be excited by electron impact having energies above 10 eV and the cross sections for electronic excitation are not always small compared to that of rotational excitation [41]. The excitation mechanisms are widely different depending upon the electron energy. With the laser-generated electron pulses as sources of high-energy electron beams such measurements can be extended to a wider domain. Moreover the observation of high-current prompt electron emission sheds more light on its role on plasma shielding which hitherto was considered as appreciable only in ps laser interactions. Another important application which may arise is in the rotational–vibrational spectroscopy of volatile molecules. The small temporal width of the electron pulses can effectively be used for vibrational relaxation experiments to measure the various rate constants.

Acknowledgements. The authors wish to acknowledge financial assistance received from the Department of Science and Technology (Government of India). RCI and PG are thankful to the University Grants Commission (New Delhi) for research fellowships.

References

1. D.B. Chrisey, G.K. Hubler (Eds.): *Pulsed Laser Deposition of Thin Films* (Wiley, New York 1994)
2. J.C. Miller, D.B. Geohegan (Eds.): *Laser Ablation, Mechanisms and Applications - II* (American Institute of Physics, New York 1994)
3. K.L. Saegner: Proc. Adv. Mater. **3**, 63 (1993)
4. D.H. Lowndes, D.B. Geohegan, A.A. Puretzky, D.P. Norton, C.M. Rouleau: Science **273**, 898 (1996)
5. Y. Lida: Spectrochim. Acta B **45**, 1353 (1990)
6. R. Kelly, B. Braren: Appl. Phys. B **53**, 160 (1991)
7. S.I. Anisimov, D. Bauerle, B.S. Luk'yanchuk: Phys. Rev. B **48**, 12 076 (1993)
8. P.P. Pronko, S.K. Dutta, D. Du, R.K. Singh: J. Appl. Phys. **78**, 6233 (1995)
9. J. Gonzalo, C.N. Afonso, I. Madariaga: J. Appl. Phys. **81**, 951 (1997)
10. R.K. Singh, J. Narayan: Phys. Rev. B **41**, 8843 (1990)
11. J.M. Ballesteros, C.N. Afonso, J. Perriere: Appl. Surf. Sci. **109/110**, 322 (1997)
12. R.C. Issac, K. Vasudevan Pillai, S.S. Harilal, G.K. Varier, C.V. Bindhu, P. Gopinath, P. Radhakrishnan, V.P.N. Nampoori, C.P.G. Vallabhan: Appl. Surf. Sci. **125**, 227 (1998)
13. R.W. Dreyfus: J. Appl. Phys. **69**, 1721 (1991)
14. G. Hatem, C. Colon, J. Campose: Spectrochim. Acta A **49**, 509 (1993)
15. P. Verardi, M. Dinescu, C. Gerardi, L. Mirenghi, V. Sandu: Appl. Surf. Sci. **109/110**, 371 (1997)
16. H.E. Elsayed - Ali, T.B. Norris, M.A. Pessot, G.A. Mourou: Phys. Rev. Lett. **58**, 1212 (1987)
17. S. Eliezer, H. Hora: Phys. Rep. **172**, 339 (1989)
18. R.W. Dreyfus, A. Phipps, A. Vertes: *Laser Ablation, Mechanisms and Applications - II*, ed. by J.C. Miller and D.B. Geohegan (AIP Conference Proceedings, American Institute of Physics, New York 1993) p. 288
19. J.F. Fujimoto, J.M. Liu, E.P. Ippen, N. Bloembergen: Phys. Rev. Lett. **53**, 1837 (1984)
20. G.L. Eesley: Phys. Rev. Lett. **51**, 2140 (1983)
21. G.L. Eesley: Phys. Rev. B **33**, 2144 (1986)
22. G. Farkas, C. Toth: Phys. Rev. A **41**, 4123 (1990)
23. S.D. Moustaizis, M. Tatarakis, C. Kalpouzos, C. Fotakis: Appl. Phys. Lett. **60**, 1939 (1992)
24. T. Hauser, W. Scheid, H. Hora: Phys. Lett. A **186**, 189 (1994)
25. R.C. Weast (Ed.): *CRC Handbook of Chemistry and Physics* (CRC Press, Florida 1988)
26. H. Cronberg, H. Reichling, E. Broberg, H.B. Nielsen, E. Mathias, N. Tolk: Appl. Phys. B **52**, 155 (1991)
27. R.E. Russo: Appl. Spectrosc. **49**, 14A (1995)
28. R.R. Freeman, T.J. Mcllrath, P.J. Bucksbaum, M. Bushkamsky: Phys. Rev. Lett. **57**, 3156 (1986)
29. T.W.B. Kibble: Phys. Rev. **150**, 1060 (1966)
30. B.S. Yilbas, Z. Yilbas, N.A. Akiakoyun: Opt. Laser Tech. **28**, 503 (1996)
31. T. Kerdja, S. Abelelli, D. Ghobrini, S. Malik: J. Appl. Phys. **80**, 5365 (1996)
32. R.C. Issac, S.S. Harilal, C.V. Bindhu, G.K. Varier, V.P.N. Nampoori, C.P.G. Vallabhan: Spectrochim. Acta B **52**, 1791 (1997)
33. G.K. Varier, R.C. Issac, S.S. Harilal, C.V. Bindhu, V.P.N. Nampoori, C.P.G. Vallabhan: Spectrochimica Acta B **52**, 657 (1997)
34. E.W. Thomas: *Excitations in Heavy Particle Collisions* (Wiley Interscience, New York 1972)
35. G. Herzberg: *Spectra of Diatomic Molecules* (Van Nostrand, New York 1961) p. 209
36. R.P. Lowe, H.I.S. Fergusson: Proc. Phys. Soc. (London) **85**, 813 (1965)
37. J.H. Moore Jr., J.P. Doering: Phys. Rev. **174**, 178 (1968)
38. H.R. Griem: *Plasma Spectroscopy* (McGraw Hill, New York 1964)
39. S.S. Harilal, C.V. Bindhu, R.C. Issac, V.P.N. Nampoori, C.P.G. Vallabhan: J. Appl. Phys. **82**, 2140 (1997)
40. A. Bourden, V. Vervish: Phys. Rev. E **55**, 4634 (1997)
41. Y. Itikawa, M. Hayashi, A. Ichimura, K. Onda, K. Sakimoto, K. Takayanagi, M. Nakamura, H. Nishimura, T. Takayanagi: J. Phys. Chem. Ref. Data **15**, 985 (1986)